

# Modulation of electronic and thermal proprieties of TaMoS<sub>2</sub> by controlling the repulsive interaction between Ta dopant atoms

Nzar Rauf Abdullah<sup>a,b</sup>, Botan Jawdat Abdullah<sup>c</sup>, Hunar Omar Rashid<sup>a</sup>, Chi-Shung Tang<sup>d</sup>, Vidar Gudmundsson<sup>e</sup>

<sup>a</sup>*Division of Computational Nanoscience, Physics Department, College of Science, University of Sulaimani, Sulaimani 46001, Kurdistan Region, Iraq*

<sup>b</sup>*Computer Engineering Department, College of Engineering, Komar University of Science and Technology, Sulaimani 46001, Kurdistan Region, Iraq*

<sup>c</sup>*Physics Department, College of Science- Salahaddin University-Erbil*

<sup>d</sup>*Department of Mechanical Engineering, National United University, 1, Lienda, Miaoli 36003, Taiwan*

<sup>e</sup>*Science Institute, University of Iceland, Dunhaga 3, IS-107 Reykjavik, Iceland*

---

## Abstract

We theoretically study the electronic and the thermal characteristics of Tantalum, Ta, doped Molybdenum disulfide, MoS<sub>2</sub>, using density functional theory. It has been shown that the MoS<sub>2</sub> monolayer is not a good material for thermoelectric devices due to its relatively large band gap. We find that a Ta doped MoS<sub>2</sub> forming a TaMoS<sub>2</sub> monolayer can be useful for thermoelectric devices. The particular attention of this work is paid to the interaction effect between the Ta atoms in the MoS<sub>2</sub> structure. We find that the interaction type is repulsive. It introduces an asymmetry in the density of states, DOS, reducing the band gap. In the presence of a strong repulsive interaction of Ta-Ta atoms, new states in the DOS around the Fermi energy are found leading to a reduction of the band gap. Consequently, a high Seebeck coefficient and figure of merit are seen over a wide range of energy around the Fermi energy. In contrast, a small reduction of the band gap and a vanishing degeneracy of the valence and the conduction bands are observed for the case of a weak Ta-Ta repulsive interaction leading to less promising thermoelectric properties.

*Keywords:* Thermoelectric, MoS<sub>2</sub>, DFT, Electronic structure,, Doping

---

Two-dimensional (2D) transition metal dichalcogenides (TMDs) materials are attracting a significant deal of interest due to their unique properties and great potential for applications in nanotechnology [1, 2, 3]. Among all 2D TMDs, Molybdenum disulfide (MoS<sub>2</sub>) has turned out to be one of the most interesting materials for applications due to a series of special and tunable physical and chemical properties [4, 5, 6] in various fields with potential as field-effect transistors [7], solar energy devices [8], energy conversion [9] and energy storage devices [10], photoluminescence [11], catalysis for hydrogen evolution reaction [12], piezoelectric devices [13], photo-electro catalysis [14, 15] electrical-thermal conductivity [16, 17] and sensor technologies [18, 19].

More significantly, a monolayer MoS<sub>2</sub> has a large direct band gap of 1.8 eV, whereas a bulk crystal has an indirect gap semiconductor with a band gap of 1.29 eV [20, 21]. Therefore, 2D MoS<sub>2</sub> has a superior electric performance calling for more attention among the 2D TMDs materials. Doping nanomaterials provides an additional flexibility to change their characteristics. Lately, the dependence of the physical properties on the system size have been studied experimentally and theoretically for both pure and doped

form of 2D materials as it provides a flexible way to alter the properties of materials for different applications. Transition elements have been used for doping 2D-TMDCs.

There are several recent theoretical studies predicting specific properties of MoS<sub>2</sub> monolayers with different dopants. A MoS<sub>2</sub> monolayer with doped Re and Nb can lead to both n-type and p-type conductivity according to DFT-LSDA calculations [22]. A DFT-LDA modeling shows that the dielectric environment of a MoS<sub>2</sub> monolayer affects the transition atom states leading to shallow energy levels [23]. The Re and Au dopants have been shown to be dispersed or aggregated in the MoS<sub>2</sub> layers providing catalytically active sites within a spin polarized DFT, Ti and V dopants enhance the electrical conductivity and photo-sensitivity of MoS<sub>2</sub> according to a DFT-GGA calculation [24, 25]. DFT calculations of the change in the Gibbs free energy in relation to hydrogen adsorption indicate that the basal plane of the distorted tetragonal structured alloy catalyst becomes active for hydrogen evolution reaction when alloyed with Ra [26]. DFT calculations at the GGA level predict that a MoS<sub>2</sub> monolayer is nonmagnetic and is energy favorable for ferromagnetic coupling with Co dopants inducing spin polarized states around the Fermi energy [1]. Ni doped MoS<sub>2</sub> monolayer has been proposed as a novel gas adsorbent to remove the typical decomposition components of H<sub>2</sub>S and SO<sub>2</sub> molecules interacting

---

*Email address:* nzar.r.abdullah@gmail.com (Nzar Rauf Abdullah)

with the Ni-MoS<sub>2</sub> surface based on DFT-GGA calculation [27]. The effects of V dopants on the antiferromagnetic and the ferromagnetic states of a monolayer MoS<sub>2</sub> depend on the separation between the V dopants was found in a DFT-GGA calculation[28]. Furthermore, Mn, Fe, Co, V, Nb and Ta have been used as dopants in MoS<sub>2</sub> monolayers to investigate the electronic properties within a DFT at the GGA level and the results indicated that the impurity elements have very low formation energies for their substitution of a Mo atom achieving the most negative value for Ta [29]. Choi has shown how strain changes electronic properties of p doped MoS<sub>2</sub> with Nb and Ta through first-principles hybrid functional calculations [30].

In this work, a monolayer MoS<sub>2</sub> doped with Ta is investigated and the obtained results of the DFT-GGA calculations are analyzed to further predict the electronic and thermal properties [31]. The effects of the repulsive interaction between the dopant Ta atoms in the MoS<sub>2</sub> monolayer are considered and how they can be used to tune the electronic and thermal properties. This tuning possibility has not reported previously. Especially, we find a high figure of merit, ZT, due to a change in the electrical conductivity, thermal conductivity and Seebeck coefficient [32]. This study reveals that Ta doping of MoS<sub>2</sub> can have a novel impact on the electronic and thermal properties of MoS<sub>2</sub> monolayers.

In Sec. 1 the computational tools are shown. In Sec. 2 the main achieved results are analyzed. In Sec. 3 the conclusion of results is presented.

## 1. Computational Tools

To model and visualize the structures under investigation, we use XCrySDen and VESTA [33, 34]. The density functional theory (DFT) implemented in Quantum espresso (QE) package is used to study the physical properties of the systems [35, 36]. A projector augmented wave (PAW) potential is utilized to treat the electron-ion interactions and the valence electrons are evaluated explicitly with a plane-wave basis set with a cutoff energy of 1088.45 eV [37]. The Perdew-Burke-Ernzerhof (PBE) functional is used to calculate the exchange-correlation energy. The structures are considered fully relaxed on a  $14 \times 14 \times 1$   $k$ -mesh grid when the changes in energy and forces are less than  $10^{-8}$  eV and  $10^{-5}$  eV/Å, respectively [37].

A convergence criteria for the energy of the Self-Consistent Field (SCF) is tested on the  $14 \times 14 \times 1$   $k$ -mesh grid, but for the density of states (DOS) calculation a  $100 \times 100 \times 1$   $k$ -mesh is utilized. All the structures are simulated with spacers of 20 Å of vacuum on either side of the 2d-structure in order to avoid interaction between charge images in the sheets.

Finally, to calculate thermometric characteristics, the Boltzmann transport properties software package (BoltzTraP) is used [38]. The BoltzTraP code uses a mesh of band energies and has an interface to the QE package [39, 40].

## 2. Results

We consider a  $2 \times 2$  supercell for the MoS<sub>2</sub> and the Ta doped MoS<sub>2</sub> monolayers. The Ta atoms in MoS<sub>2</sub> do energetically interact with each other, and the interaction effects influence the physical properties of the material. The analysis of the effects of the Ta-Ta interactions on the TaMoS<sub>2</sub> monolayers must be based on a comparison to a pristine MoS<sub>2</sub> monolayer. Because of that we briefly revise the electronic and the thermal properties of a MoS<sub>2</sub> monolayer.

The unit cell of a MoS<sub>2</sub> layer consists of 6 atoms; two molybdenum (Mo) atoms are located at the Wyckoff  $2c$  sites and four sulfur (S) atoms at the Wyckoff  $4f$  sites [41]. So a  $2 \times 2$  supercell single layer of MoS<sub>2</sub> contains four Mo and eight S atoms as is shown in the parallelogram of Fig. 1(a). The bonding type is mainly covalent within the atomically thin S-Mo-S layers. In our calculation of MoS<sub>2</sub> monolayer, the obtained bond length between Mo-S atoms and the lattice constant are 2.41 Å, and 3.18 Å, respectively. These are very close to experimental values of Mo-S bond length, 2.383 Å, and lattice constant, 3.16 Å [41]. The bond angles of the Mo-S-Mo and S-Mo-S in the pure MoS<sub>2</sub> monolayer are both 82.55°, with 81.55° being theoretically obtained earlier [42]. The separation between sulfur layers is 3.126 Å, which can be compared to the experimental value, 3.18 Å, measured by means of STM images.

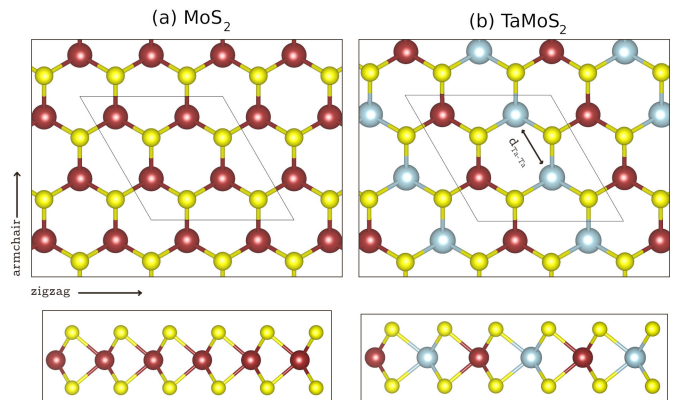


Figure 1: Pure MoS<sub>2</sub> monolayer (a), and Ta-doped MoS<sub>2</sub> monolayer (b) of both top view (top panels), and side view (bottom panels). The Mo, S and Ta atoms are colored brown, yellow, and cyan, respectively.

In the Ta-doped MoS<sub>2</sub> system identified as the TaMoS<sub>2</sub> structure (see Fig. 1b), four atomic configurations based on the distance between the Ta atoms,  $d_{\text{Ta-Ta}}$ , are considered. The concentration of the Ta dopant atoms is assumed to be 16.6% corresponding to two Ta atoms doped in the  $2 \times 2$  supercell of the MoS<sub>2</sub> structure. The distance between the two Ta atoms are 2.56, 3.01, 4.14, and 4.47 Å in the four atomic configurations, identified as TaMoS<sub>2</sub>-1, TaMoS<sub>2</sub>-2, TaMoS<sub>2</sub>-3, and TaMoS<sub>2</sub>-4 structures, respectively. The two Ta atoms are substitutionally doped in the

MoS<sub>2</sub> structures in such a way that one Ta is exchanged for a Mo atom while the other one replaces an S atom in all four atomic configurations. In this way, we can keep the semiconductor behavior of the TaMoS<sub>2</sub> with a finite bandgap.

The four configurations of TaMoS<sub>2</sub> with different distances between Ta atoms gives different interaction strength between the dopant atoms. The interaction energy can be defined as [43, 44]

$$E_{\text{int}} = E_2 - E_0 + 2 \times E_1, \quad (1)$$

where  $E_0$ ,  $E_1$  and  $E_2$  are the total energies of the systems with zero, one and two substitutional dopant Ta atoms, respectively. We found that the interaction is repulsive as the interaction energy has a positive value for all the four considered configurations. The repulsive energy is plotted as a function of the distance between the Ta atoms in Fig. 2. One can see that as the distance between the Ta atoms is increased the repulsive interaction between the dopant atoms is decreased. TaMoS<sub>2</sub>-1 has the strongest attractive interaction while TaMoS<sub>2</sub>-4 has the weakest attractive interaction among the considered TaMoS<sub>2</sub> structures.

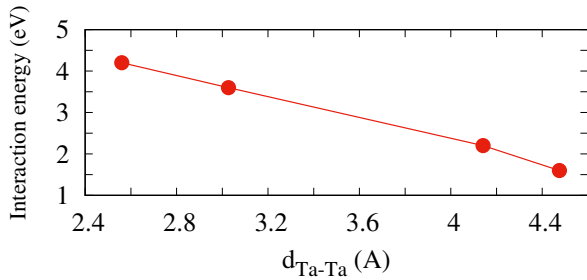


Figure 2: Interaction energy,  $E_{\text{int}}$ , between the Ta atoms versus the distance between the Ta atoms,  $d_{\text{Ta-Ta}}$

The attractive interaction between the Ta dopant atoms modifies the Mo-S, and Mo-Ta bond lengths, and the bond angles of Mo-S-Mo and S-Mo-S as is presented in Tab. 1. We can clearly see that the stronger repulsive interaction between Ta atoms increases the lattice constant of the TaMoS<sub>2</sub> structure. So, the TaMoS<sub>2</sub>-1(TaMoS<sub>2</sub>-4) has the longest(shortest) lattice constant among the TaMoS<sub>2</sub> structures.

Table 1: Lattice constant,  $a$ , Mo-S-Mo bond angle, S-Mo-S bond angle, Mo-Ta, and Mo-S bond length for TaMoS<sub>2</sub> structures. The unit of all bond length is Å.

Structure	$a$	Mo-S-Mo	S-Mo-S	Mo-Ta	Mo-S
TaMoS <sub>2</sub> -1	3.327	83.819	80.585	2.560	2.444
TaMoS <sub>2</sub> -2	3.261	83.583	82.976	2.560	2.420
TaMoS <sub>2</sub> -3	3.201	83.22	82.171	2.566	2.46
TaMoS <sub>2</sub> -4	3.192	77.736	83.144	2.99	2.5

The Ta-Ta repulsive interaction elongates the unit cell

of the TaMoS<sub>2</sub> causing a high sub-lattice symmetry breaking. It thus influences the density of states and the band structures of MoS<sub>2</sub>. The partial density of state, PDOS, of the MoS<sub>2</sub> (a) and TaMoS<sub>2</sub> structures (b-e) are presented in Fig. 3. The major PDOS contribution in the pure MoS<sub>2</sub> monolayer around Fermi energy is the  $d$ -orbital of the Mo atoms (Mo- $d$ ) hybridized with the  $p$ -orbital of the S atoms (S- $p$ ). The contributions of Mo become more relevant as the energy approaches the band gap because the atomic radius of an Mo atom is larger than that of an S atom. In addition, states which come from the S- $p$  orbitals are, more importantly, 1 eV below the Fermi level.

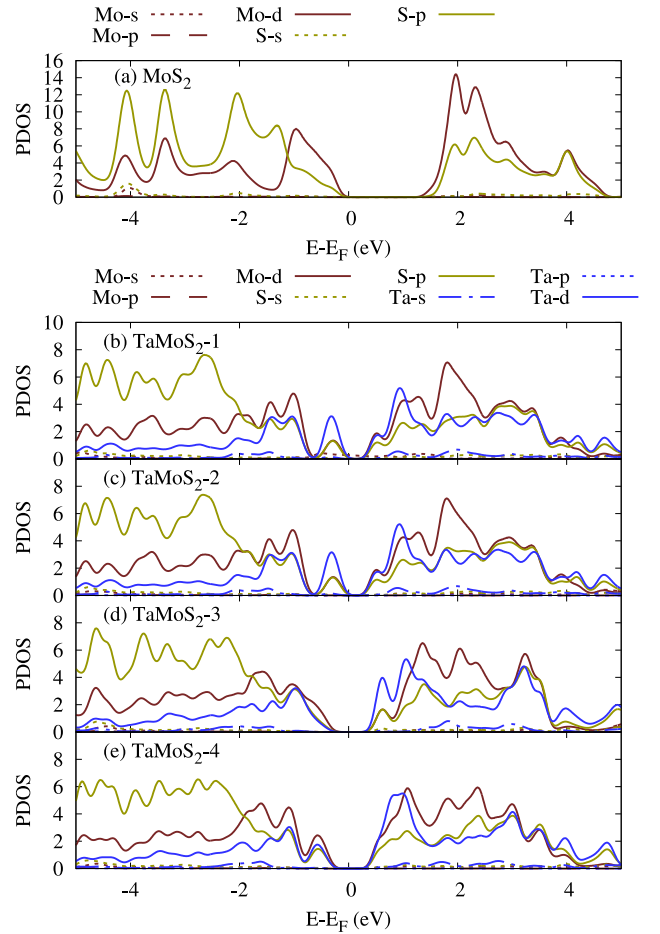


Figure 3: Partial density of states (PDOS) of the MoS<sub>2</sub> (a) and TaMoS<sub>2</sub> (b-e). The Fermi energy is set to zero.

The Mo- $s$  and the S- $s$  orbital contributions appear really deep in energy, they are not expected to play an important role in this system due to their highly stable nature. We therefore assume only Mo- $d$  and S- $p$  orbitals. Our PDOS analysis of MoS<sub>2</sub> is well in agreement with the literature [45].

In the presence of the Ta-Ta repulsive interaction, several new states are introduced near the Fermi energy. Also, a major Ta atoms rearrangement, relative to the pristine MoS<sub>2</sub> case, in the contributions of each element to the total DOS is apparent. In the presence of a strong Ta-Ta

repulsive interaction, in TaMoS<sub>2</sub>-1, a peak in the valence band region below the Fermi energy from 0 to -0.6 eV and several peaks in the conduction band region from 0 to 1.6 eV due to the Ta-Ta repulsive interaction are seen. The contribution of Ta atoms in these peaks is decreases with decreasing Ta-Ta interaction strength. This is clear in TaMoS<sub>2</sub>-4, especially in the valence band region. In contrast, with a decreasing Ta-Ta interaction strength the unoccupied states generated by the Ta atoms in the conduction band region is enhanced. Again, the *d*-orbitals of Ta atoms are the most active ones, Ta-*d* (solid blue in Fig. 3). The contribution of the Ta atoms in the density of states decreases the PDOS of the Mo and S atoms.

Another consequence of the levels introduced by the Ta-Ta interaction is the reduction of the band gap. The band structure of MoS<sub>2</sub> (a) and TaMoS<sub>2</sub> (b-e) are presented in Fig. 4. The band gap of pure MoS<sub>2</sub> monolayer is found to be direct and the band gap value is 1.68 eV at the K point which is agree with the previous results [46]. As we have seen from the PDOS, the top of valence band and the bottom of conduction band are mainly formed by the *d*-orbital of the Mo atoms in MoS<sub>2</sub> monolayer.

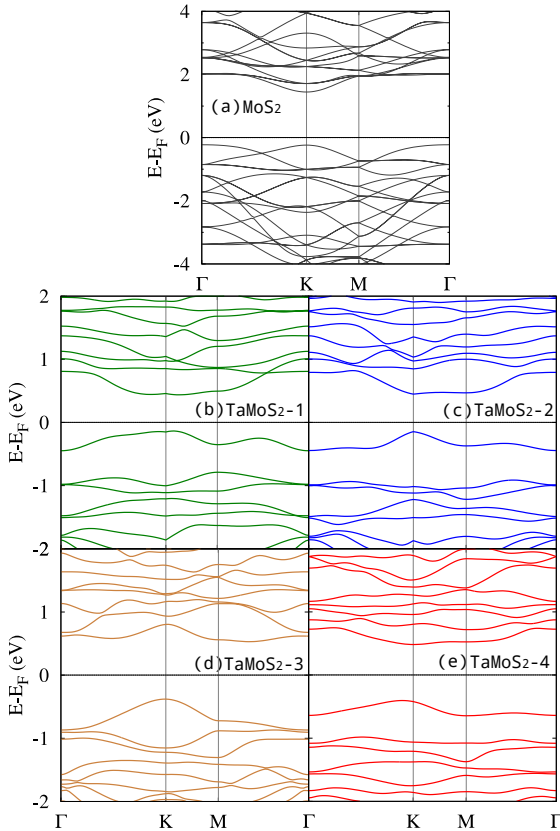


Figure 4: Band structure for optimized structures of the MoS<sub>2</sub> (a) and TaMoS<sub>2</sub> (b-e). The energies are with respect to the Fermi level, and the Fermi energy is set to zero.

In the presence of the repulsive Ta-Ta interaction in TaMoS<sub>2</sub> the band gap is reduced as states are generated in the band gap region due to the *d*-orbitals of the Ta atoms. The stronger the repulsive interaction, the smaller band

gap is seen, as can be seen from Fig. 5. The band gap values of TaMoS<sub>2</sub>-1, TaMoS<sub>2</sub>-2, TaMoS<sub>2</sub>-3, and TaMoS<sub>2</sub>-4 are 0.572, 0.594, 0.909, 0.886 eV, respectively. In addition, the degeneracy of the energy levels is reduced with decreasing Ta-Ta interaction strength in both the valence and the conduction band regions (see Fig. 4(d)).

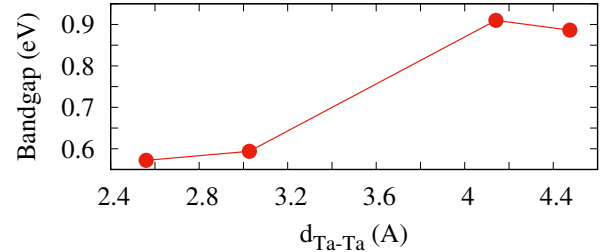


Figure 5: Band gap versus the distance between the Ta atoms,  $d_{\text{Ta-Ta}}$

The asymmetry of the band structure and the density of states caused by the Ta-Ta interaction is useful for controlling the thermoelectric properties of the systems [37]. We are interested in the investigation of the thermoelectric properties in the temperature range  $T = 20\text{-}160$  K, where the electron contribution to the transport is dominant and the phonon participation can be neglected as the electron and the lattice temperatures are decoupled in this temperature range [47, 48].

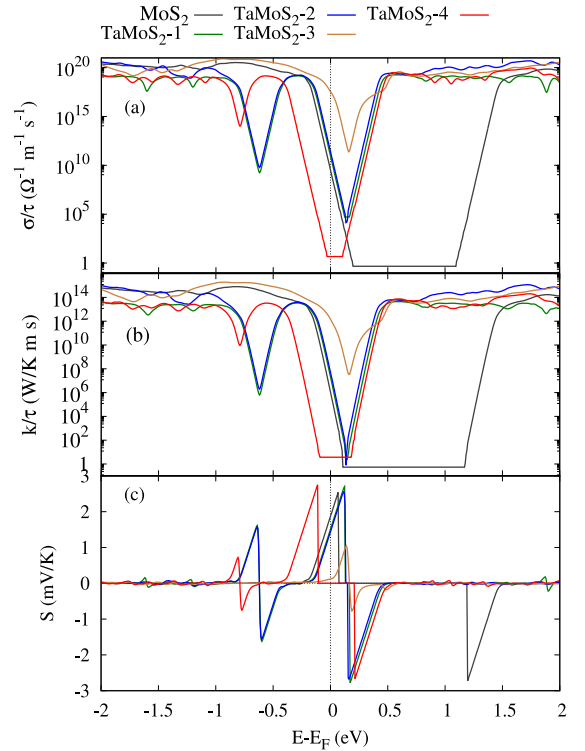


Figure 6: Electrical conductance,  $\sigma$ , (a), electronic part of thermal conductance,  $k$ , (b), and Seebeck coefficient,  $S$ , (c) versus energy for pure MoS<sub>2</sub> and TaMoS<sub>2</sub> monolayers. The Fermi energy is set to zero.

We have used the BoltzTrap code to study the thermoelectric properties of the systems. The Boltzmann theory is implemented in the BoltzTrap code, which is utilized to obtain the semiclassical transport coefficients. The code uses a mesh of band energies and is interfaced to the QE package.

There are several attempt to enhance the figure of merit,  $ZT$ , which reflects the efficiency of thermoelectric devises. The  $ZT$  can be defined as [49, 50]

$$ZT = \frac{S^2 \sigma}{k} T, \quad (2)$$

where  $S$  notes the Seebeck coefficient,  $\sigma$  is the electrical conductance,  $k$  is the thermal conductance, and  $T$  is the temperature. In order to obtain a high  $ZT$ , one has to have high values of  $S$  and  $\sigma$ , and a low value of  $k$  [51]. The  $S$  (a),  $\sigma$  (b), and  $k$  (c) as functions of energy are plotted in Fig. 6 for MoS<sub>2</sub> (a) and TaMoS<sub>2</sub> (b-e) monolayers. One can clearly see the influence of the wide band gap of MoS<sub>2</sub> on the thermoelectric properties. The values of  $\sigma$ ,  $k$ , and  $S$  are close to zero over a wide range of energy, due to the relatively large band gaps of MoS<sub>2</sub>. It produces a vanishing  $ZT$  over a wide range of energies from 0 to 1.2 eV as is shown in Fig. 7(a). We can thus confirm that the MoS<sub>2</sub> itself is not a good material for thermometric devices.

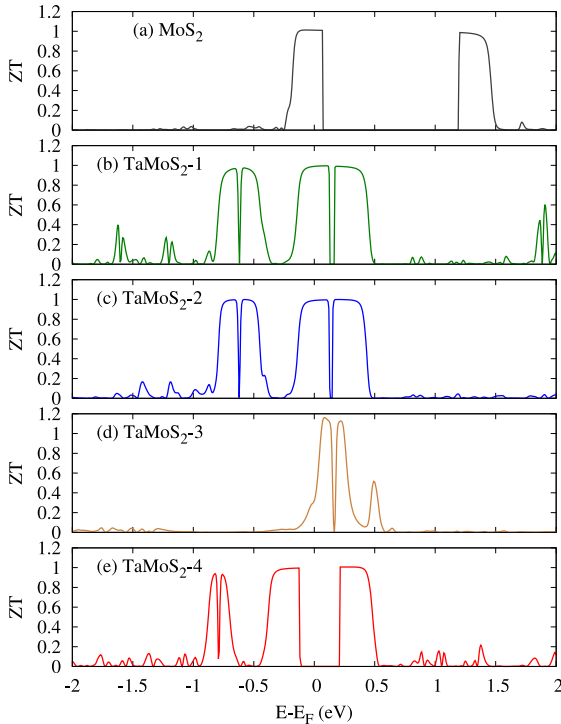


Figure 7: Figure of merit versus energy for pure MoS<sub>2</sub> (a) and TaMoS<sub>2</sub> (b-e) monolayers. The Fermi energy is set to zero.

In the presence of a repulsive Ta-Ta interaction, the enhanced symmetry of the density of states and the band structure enhance the Seebeck coefficient and thus a maximum value of  $ZT$  is found for the TaMoS<sub>2</sub>-3 in a small energy range around the Fermi energy. The value of

$ZT \approx 1.2$  for TaMoS<sub>2</sub>-3 is seen (see Fig. 7(d)). This results may be useful for thermoelectric devices.

### 3. Conclusion and Remarks

The framework of this study is based on the Kohn-Sham density functional approach to investigate electronic and thermal properties of the Tantalum doped Molybdenum disulfide monolayer. We found that the MoS<sub>2</sub> monolayer is not a good material for thermoelectric devices because of its wide band gap. To enhance its thermal behavior Ta atoms are used as dopant atoms. More precisely, we focus on the interaction effect between the Ta atoms doped in MoS<sub>2</sub> in this study. In the presence of a strong attractive interaction between Ta atoms, several new states are introduced near the Fermi energy. Consequently, the band gap is reduced in the still semiconducting TaMoS<sub>2</sub>. The reduced band gap can enhance the Seebeck coefficient and the figure of merit. In the presence of a weak Ta-Ta attractive interaction, the band gap is slightly reduced but remains large, which is promising for thermoelectric devices. We thus see vanishing Seebeck coefficient and figure of merit over a wide range of energy. Our study may be useful for thermoelectric devices such as thermoelectric generators.

### 4. Acknowledgment

This work was financially supported by the University of Sulaimani and the Research center of Komar University of Science and Technology. The computations were performed on resources provided by the Division of Computational Nanoscience at the University of Sulaimani.

### References

- [1] Y. Wang, S. Li, J. Yi, [Electronic and magnetic properties of co doped mos2 monolayer](#), Scientific Reports 6 (1) (2016) 24153. URL <https://doi.org/10.1038/srep24153>
- [2] S.-H. Kim, J. Lim, R. Sahu, O. Kasian, L. T. Stephenson, C. Scheu, B. Gault, [Direct imaging of dopant and impurity distributions in 2d mos2](#), Advanced Materials 32 (8) (2020) 1907235. [arXiv:https://onlinelibrary.wiley.com/doi/pdf/10.1002/adma.201907235](https://onlinelibrary.wiley.com/doi/pdf/10.1002/adma.201907235), doi:<https://doi.org/10.1002/adma.201907235>. URL <https://onlinelibrary.wiley.com/doi/abs/10.1002/adma.201907235>
- [3] V. Asokan, D. Zhu, W. Huang, H. Wang, W. Gao, Z. Zhang, C. Jin, [Growth of 'w' doped molybdenum disulfide on graphene transferred molybdenum substrate](#), Scientific Reports 8 (1) (2018) 7396. doi:[10.1038/s41598-018-25796-9](https://doi.org/10.1038/s41598-018-25796-9). URL <https://doi.org/10.1038/s41598-018-25796-9>
- [4] I. Song, C. Park, H. C. Choi, [Synthesis and properties of molybdenum disulphide: from bulk to atomic layers](#), RSC Adv. 5 (2015) 7495–7514. doi:[10.1039/C4RA11852A](https://doi.org/10.1039/C4RA11852A). URL <http://dx.doi.org/10.1039/C4RA11852A>
- [5] H. Xu, J. Zhu, Q. Ma, J. Ma, H. Bai, L. Chen, S. Mu, [Two-dimensional mos2: Structural properties, synthesis methods, and regulation strategies toward oxygen reduction](#), Micromachines 12 (3) (2021). doi:[10.3390/mi12030240](https://doi.org/10.3390/mi12030240). URL <https://www.mdpi.com/2072-666X/12/3/240>

- [6] N. R. Abdullah, H. O. Rashid, C.-S. Tang, A. Manolescu, V. Gudmundsson, *Modeling electronic, mechanical, optical and thermal properties of graphene-like bc<sub>6n</sub> materials: Role of prominent bn-bonds*, *Physics Letters A* 384 (32) (2020) 126807. doi:<https://doi.org/10.1016/j.physleta.2020.126807>. URL <http://www.sciencedirect.com/science/article/pii/S0375960120306745>
- [7] A. Dankert, L. Langouche, M. V. Kamalakar, S. P. Dash, *High-performance molybdenum disulfide field-effect transistors with spin tunnel contacts*, *ACS Nano* 8 (1) (2014) 476–482, pMID: 24377305. arXiv:<https://doi.org/10.1021/nn404961e>. URL <https://doi.org/10.1021/nn404961e>
- [8] D. Lembke, A. Kis, *Breakdown of high-performance monolayer mos<sub>2</sub> transistors*, *ACS Nano* 6 (11) (2012) 10070–10075, pMID: 23039374. arXiv:<https://doi.org/10.1021/nn303772b>. URL <https://doi.org/10.1021/nn303772b>
- [9] S. Wi, H. Kim, M. Chen, H. Nam, L. J. Guo, E. Meyhofer, X. Liang, *Enhancement of photovoltaic response in multilayer mos<sub>2</sub> induced by plasma doping*, *ACS Nano* 8 (5) (2014) 5270–5281, pMID: 24783942. arXiv:<https://doi.org/10.1021/nn5013429>. URL <https://doi.org/10.1021/nn5013429>
- [10] S. Ding, D. Zhang, J. S. Chen, X. W. D. Lou, *Facile synthesis of hierarchical mos<sub>2</sub> microspheres composed of few-layered nanosheets and their lithium storage properties*, *Nanoscale* 4 (2012) 95–98. doi:10.1039/C1NR11552A. URL <http://dx.doi.org/10.1039/C1NR11552A>
- [11] A. Splendiani, L. Sun, Y. Zhang, T. Li, J. Kim, C.-Y. Chim, G. Galli, F. Wang, *Emerging photoluminescence in monolayer mos<sub>2</sub>*, *Nano Letters* 10 (4) (2010) 1271–1275, pMID: 20229981. arXiv:<https://doi.org/10.1021/nl903868w>. doi:10.1021/nl903868w. URL <https://doi.org/10.1021/nl903868w>
- [12] Y. Li, H. Wang, L. Xie, Y. Liang, G. Hong, H. Dai, *Mos<sub>2</sub> nanoparticles grown on graphene: An advanced catalyst for the hydrogen evolution reaction*, *Journal of the American Chemical Society* 133 (19) (2011) 7296–7299, pMID: 21510646. arXiv:<https://doi.org/10.1021/ja201269b>. doi:10.1021/ja201269b. URL <https://doi.org/10.1021/ja201269b>
- [13] W. Wu, L. Wang, Y. Li, F. Zhang, L. Lin, S. Niu, D. Chenet, X. Zhang, Y. Hao, T. F. Heinz, J. Hone, Z. L. Wang, *Piezoelectricity of single-atomic-layer mos<sub>2</sub> for energy conversion and piezotronics*, *Nature* 514 (7523) (2014) 470–474. doi:10.1038/nature13792. URL <https://doi.org/10.1038/nature13792>
- [14] Y. Li, Y.-L. Li, C. M. Araujo, W. Luo, R. Ahuja, *Single-layer mos<sub>2</sub> as an efficient photocatalyst*, *Catal. Sci. Technol.* 3 (2013) 2214–2220. doi:10.1039/C3CY00207A. URL <http://dx.doi.org/10.1039/C3CY00207A>
- [15] F. M. Pesci, M. S. Sokolikova, C. Grotta, P. C. Sherrell, F. Reale, K. Sharda, N. Ni, P. Palczynski, C. Mattevi, *Mos<sub>2</sub>/ws<sub>2</sub> heterojunction for photoelectrochemical water oxidation*, *ACS Catalysis* 7 (8) (2017) 4990–4998. arXiv:<https://doi.org/10.1021/acscatal.7b01517>. doi:10.1021/acscatal.7b01517. URL <https://doi.org/10.1021/acscatal.7b01517>
- [16] M.-J. Lee, J.-H. Ahn, J. H. Sung, H. Heo, S. G. Jeon, W. Lee, J. Y. Song, K.-H. Hong, B. Choi, S.-H. Lee, M.-H. Jo, *Thermoelectric materials by using two-dimensional materials with negative correlation between electrical and thermal conductivity*, *Nature Communications* 7 (1) (2016) 12011. doi:10.1038/ncomms12011. URL <https://doi.org/10.1038/ncomms12011>
- [17] N. R. Abdullah, M. T. Kareem, H. O. Rashid, A. Manolescu, V. Gudmundsson, *Spin-polarised dft modeling of electronic, magnetic, thermal and optical properties of silicene doped with transition metals*, *Physica E: Low-dimensional Systems and Nanostructures* 129 (2021) 114644. doi:<https://doi.org/10.1016/j.physe.2021.114644>. URL <https://www.sciencedirect.com/science/article/pii/S1386947721000266>
- [18] C. W. Lee, J. M. Suh, H. W. Jang, *Chemical sensors based on two-dimensional (2d) materials for selective detection of ions and molecules in liquid*, *Frontiers in Chemistry* 7 (2019) 708. doi:10.3389/fchem.2019.00708. URL <https://www.frontiersin.org/article/10.3389/fchem.2019.00708>
- [19] M. Donarelli, L. Ottaviano, *2d materials for gas sensing applications: A review on graphene oxide, mos<sub>2</sub>, ws<sub>2</sub> and phosphorene*, *Sensors* 18 (11) (2018). doi:10.3390/s18113638. URL <https://www.mdpi.com/1424-8220/18/11/3638>
- [20] K. F. Mak, C. Lee, J. Hone, J. Shan, T. F. Heinz, *Atomically thin mos<sub>2</sub>: A new direct-gap semiconductor*, *Phys. Rev. Lett.* 105 (2010) 136805. doi:10.1103/PhysRevLett.105.136805. URL <https://link.aps.org/doi/10.1103/PhysRevLett.105.136805>
- [21] G. L. Frey, S. Elani, M. Homyonfer, Y. Feldman, R. Tenne, *Optical-absorption spectra of inorganic fullerene-like ms<sub>2</sub> (m = Mo, w)*, *Phys. Rev. B* 57 (1998) 6666–6671. doi:10.1103/PhysRevB.57.6666. URL <https://link.aps.org/doi/10.1103/PhysRevB.57.6666>
- [22] K. Dolui, I. Rungger, C. Das Pemmaraju, S. Sanvito, *Possible doping strategies for mos<sub>2</sub> monolayers: An ab initio study*, *Phys. Rev. B* 88 (2013) 075420. doi:10.1103/PhysRevB.88.075420. URL <https://link.aps.org/doi/10.1103/PhysRevB.88.075420>
- [23] J.-Y. Noh, H. Kim, M. Park, Y.-S. Kim, *Deep-to-shallow level transition of re and nb dopants in monolayer mos<sub>2</sub> with dielectric environments*, *Phys. Rev. B* 92 (2015) 115431. doi:10.1103/PhysRevB.92.115431. URL <https://link.aps.org/doi/10.1103/PhysRevB.92.115431>
- [24] I. Williamson, S. Li, A. Correa Hernandez, M. Lawson, Y. Chen, L. Li, *Structural, electrical, phonon, and optical properties of ti- and v-doped two-dimensional mos<sub>2</sub>*, *Chemical Physics Letters* 674 (2017) 157–163. doi:<https://doi.org/10.1016/j.cplett.2017.02.053>. URL <https://www.sciencedirect.com/science/article/pii/S0009261417301707>
- [25] N. R. Abdullah, H. O. Rashid, M. T. Kareem, C.-S. Tang, A. Manolescu, V. Gudmundsson, *Effects of bonded and non-bonded b/n codoping of graphene on its stability, interaction energy, electronic structure, and power factor*, *Physics Letters A* 384 (12) (2020) 126350. doi:10.1016/j.physleta.2020.126350. URL <http://www.sciencedirect.com/science/article/pii/S0375960120301602>
- [26] S.-Z. Yang, Y. Gong, P. Manchanda, Y.-Y. Zhang, G. Ye, S. Chen, L. Song, S. T. Pantelides, P. M. Ajayan, M. F. Chisholm, W. Zhou, *Rhenium-doped and stabilized mos<sub>2</sub> atomic layers with basal-plane catalytic activity*, *Advanced Materials* 30 (51) (2018) 1803477. arXiv:<https://onlinelibrary.wiley.com/doi/pdf/10.1002/adma.201803477>. doi:<https://doi.org/10.1002/adma.201803477>. URL <https://onlinelibrary.wiley.com/doi/abs/10.1002/adma.201803477>
- [27] H. Wei, Y. Gui, J. Kang, W. Wang, C. Tang, *A dft study on the adsorption of h<sub>2</sub>s and so<sub>2</sub> on ni doped mos<sub>2</sub> monolayer*, *Nanomaterials* 8 (9) (2018). doi:10.3390/nano8090646. URL <https://www.mdpi.com/2079-4991/8/9/646>
- [28] Y. Miao, Y. Li, Q. Fang, Y. Huang, Y. Sun, K. Xu, F. Ma, P. K. Chu, *Effects of dopant separation on electronic states and magnetism in monolayer mos<sub>2</sub>*, *Applied Surface Science* 428 (2018) 226–232. doi:<https://doi.org/10.1016/j.apsusc.2017.09.128>. URL <https://www.sciencedirect.com/science/article/pii/S0169433217327769>
- [29] S.-C. Lu, J.-P. Leburton, *Electronic structures of defects and magnetic impurities in mos<sub>2</sub> monolayers*, *Nanoscale Research*

- Letters 9 (1) (2014) 676. doi:10.1186/1556-276X-9-676.  
URL <https://doi.org/10.1186/1556-276X-9-676>
- [30] M. Choi, **Strain-enhanced  $p$  doping in monolayer  $\text{mos}_2$** , Phys. Rev. Applied 9 (2018) 024009. doi:10.1103/PhysRevApplied.9.024009.  
URL <https://link.aps.org/doi/10.1103/PhysRevApplied.9.024009>
- [31] N. R. Abdullah, H. O. Rashid, C.-S. Tang, A. Manolescu, V. Gudmundsson, **Properties of  $\text{bsi6n}$  monolayers derived by first-principle computation**, Physica E: Low-dimensional Systems and Nanostructures (2020) 114556 doi:https://doi.org/10.1016/j.physe.2020.114556.  
URL <http://www.sciencedirect.com/science/article/pii/S1386947720316246>
- [32] H. O. Rashid, N. R. Abdullah, V. Gudmundsson, **Silicon on a graphene nanosheet with triangle- and dot-shape: Electronic structure, specific heat, and thermal conductivity from first-principle calculations**, Results in Physics 15 (2019) 102625. doi:10.1016/j.rinp.2019.102625.  
URL <http://www.sciencedirect.com/science/article/pii/S2211379719317140>
- [33] A. Kokalj, **Xcrysden—a new program for displaying crystalline structures and electron densities**, Journal of Molecular Graphics and Modelling 17 (3) (1999) 176–179. doi:10.1016/S1093-3263(99)00028-5.  
URL <http://www.sciencedirect.com/science/article/pii/S1093326399000285>
- [34] K. Momma, F. Izumi, **Vesta 3 for three-dimensional visualization of crystal, volumetric and morphology data**, Journal of applied crystallography 44 (6) (2011) 1272–1276.
- [35] P. Giannozzi, S. Baroni, N. Bonini, M. Calandra, R. Car, C. Cavazzoni, D. Ceresoli, G. L. Chiarotti, M. Cococcioni, I. Dabo, A. D. Corso, S. de Gironcoli, S. Fabris, G. Fratesi, R. Gebauer, U. Gerstmann, C. Gougousis, A. Kokalj, M. Lazzeri, L. Martin-Samos, N. Marzari, F. Mauri, R. Mazzarello, S. Paolini, A. Pasquarello, L. Paulatto, C. Sbraccia, S. Scandolo, G. Sclauzero, A. P. Seitsonen, A. Smogunov, P. Umari, R. M. Wentzcovitch, **QUANTUM ESPRESSO: a modular and open-source software project for quantum simulations of materials**, Journal of Physics: Condensed Matter 21 (39) (2009) 395502. doi:10.1088/0953-8984/21/39/395502.  
URL <https://doi.org/10.1088/0953-8984/21/39/395502>
- [36] P. Giannozzi, O. Andreussi, T. Brumme, O. Bunau, M. B. Nardelli, M. Calandra, R. Car, C. Cavazzoni, D. Ceresoli, M. Cococcioni, et al., **Advanced capabilities for materials modelling with quantum espresso**, Journal of Physics: Condensed Matter 29 (46) (2017) 465901.
- [37] N. R. Abdullah, H. O. Rashid, A. Manolescu, V. Gudmundsson, **Interlayer interaction controlling the properties of ab- and a-stacked bilayer graphene-like  $\text{bc14n}$  and  $\text{si2c14}$** , Surfaces and Interfaces 21 (2020) 100740. doi:https://doi.org/10.1016/j.surfin.2020.100740.  
URL <http://www.sciencedirect.com/science/article/pii/S246802302030732X>
- [38] G. K. H. Madsen, D. J. Singh, **Boltztrap. a code for calculating band-structure dependent quantities**, Computer Physics Communications 175 (1) (2006) 67–71.  
URL <http://www.sciencedirect.com/science/article/pii/S0010465506001305>
- [39] N. R. Abdullah, H. O. Rashid, V. Gudmundsson, **Study of  $\text{bc14n}$ -bilayer graphene: Effects of atomic spacing and inter-atomic interaction between b and n atoms**, Superlattices and Microstructures 156 (2021) 106981. doi:https://doi.org/10.1016/j.spmi.2021.106981.  
URL <https://www.sciencedirect.com/science/article/pii/S0749603621001798>
- [40] N. R. Abdullah, H. O. Rashid, C.-S. Tang, A. Manolescu, V. Gudmundsson, **Role of interlayer spacing on electronic, thermal and optical properties of  $\text{bn}$ -codoped bilayer graphene: Influence of the interlayer and the induced dipole-dipole interactions**, Journal of Physics and Chemistry of Solids 155 (2021) 110095. doi:https://doi.org/10.1016/j.jpcs.2021.110095.  
URL <https://www.sciencedirect.com/science/article/pii/S002236972100161X>
- [41] A. Molina-Sánchez, K. Hummer, L. Wirtz, **Vibrational and optical properties of  $\text{mos}_2$ : From monolayer to bulk**, Surface Science Reports 70 (4) (2015) 554–586. doi:https://doi.org/10.1016/j.surfrep.2015.10.001.  
URL <https://www.sciencedirect.com/science/article/pii/S016757291500028X>
- [42] Y. Gui, W. Chen, Y. Lu, C. Tang, L. Xu, **Au catalyst-modified  $\text{mos}_2$  monolayer as a highly effective adsorbent for  $\text{so}_2/\text{f}_2$  gas: A dft study**, ACS Omega 4 (7) (2019) 12204–12211. arXiv:https://doi.org/10.1021/acsomega.9b01429, doi:10.1021/acsomega.9b01429.  
URL <https://doi.org/10.1021/acsomega.9b01429>
- [43] N. Al-Aqtash, K. M. Al-Tarawneh, T. Tawalbeh, I. Vasiliev, **Ab initio study of the interactions between boron and nitrogen dopants in graphene**, Journal of Applied Physics 112 (3) (2012) 034304. arXiv:https://doi.org/10.1063/1.4742063, doi:10.1063/1.4742063.  
URL <https://doi.org/10.1063/1.4742063>
- [44] N. R. Abdullah, B. J. Abdullah, C.-S. Tang, V. Gudmundsson, **Properties of  $\text{bc6n}$  monolayer derived by first-principle computation: Influences of interactions between dopant atoms on thermoelectric and optical properties**, Materials Science in Semiconductor Processing 135 (2021) 106073. doi:https://doi.org/10.1016/j.mssp.2021.106073.  
URL <https://www.sciencedirect.com/science/article/pii/S1369800121004182>
- [45] A. Mirahrio, E. Rangel Cortes, M. Castro, **Electronic properties and enhanced reactivity of  $\text{mos}_2$  monolayers with substitutional gold atoms embedded into sulfur vacancies**, Applied Surface Science 455 (2018) 758–770. doi:https://doi.org/10.1016/j.apsusc.2018.05.220.  
URL <https://www.sciencedirect.com/science/article/pii/S0169433218315472>
- [46] J. Ryou, Y.-S. Kim, S. KC, K. Cho, **Monolayer  $\text{mos}_2$  bandgap modulation by dielectric environments and tunable bandgap transistors**, Scientific Reports 6 (1) (2016) 29184. doi:10.1038/srep29184.  
URL <https://doi.org/10.1038/srep29184>
- [47] S. Yiğen, V. Tayari, J. O. Island, J. M. Porter, A. R. Champagne, **Electronic thermal conductivity measurements in intrinsic graphene**, Phys. Rev. B 87 (2013) 241411. doi:10.1103/PhysRevB.87.241411.  
URL <https://link.aps.org/doi/10.1103/PhysRevB.87.241411>
- [48] N. R. Abdullah, G. A. Mohammed, H. O. Rashid, V. Gudmundsson, **Electronic, thermal, and optical properties of graphene like six structures: Significant effects of si atom configurations**, Physics Letters A 384 (24) (2020) 126578. doi:https://doi.org/10.1016/j.physleta.2020.126578.  
URL <http://www.sciencedirect.com/science/article/pii/S037596012030445X>
- [49] J. Wang, X. Mu, M. Sun, **The thermal, electrical and thermoelectric properties of graphene nanomaterials**, Nanomaterials 9 (2) (2019). doi:10.3390/nano9020218.  
URL <https://www.mdpi.com/2079-4991/9/2/218>
- [50] A. J. Minnich, M. S. Dresselhaus, Z. F. Ren, G. Chen, **Bulk nanostructured thermoelectric materials: current research and future prospects**, Energy Environ. Sci. 2 (2009) 466–479. doi:10.1039/B822664B.  
URL <https://dx.doi.org/10.1039/B822664B>
- [51] N. R. Abdullah, **Outstanding performance of  $\text{si}$ -bilayer graphene using first-principle computation: Significant effects of  $\text{si}$  atoms configuration**, Physica B: Condensed Matter 620 (2021) 413273. doi:https://doi.org/10.1016/j.physb.2021.413273.  
URL <https://www.sciencedirect.com/science/article/pii/S0921452621004464>